nature physics

LETTERS

https://doi.org/10.1038/s41567-019-0494-8

Polarization and entanglement in baryon–antibaryon pair production in electron–positron annihilation

The BESIII Collaboration*

Particles directly produced at electron–positron colliders, such as the J/ψ meson, decay with relatively high probability into a baryon–antibaryon pair[1]. For spin-1/2 baryons, the pair can have the same or opposite helicites. A non-vanishing phase $\Delta\Phi$ between the transition amplitudes to these helicity states results in a transverse polarization of the baryons[2–4]. From the joint angular distribution of the decay products of the baryons, this phase as well as the parameters characterizing the baryon and the antibaryon decays can be determined. Here, we report the measurement of $\Delta\Phi = 42.4 \pm 0.6 \pm 0.5°$ using $\Lambda \to p\pi^-$ and $\overline{\Lambda} \to \overline{p}\pi^+$, $\overline{n}\pi^0$ decays at BESIII. We find a value for the $\Lambda \to p\pi^-$ decay parameter of $\alpha_- = 0.750 \pm 0.009 \pm 0.004$, $17 \pm 3\%$ higher than the current world average, which has been used as input for all Λ polarization measurements since 1978[5,6]. For $\overline{\Lambda} \to \overline{p}\pi^+$ we find $\alpha_+ = -0.758 \pm 0.010 \pm 0.007$, giving $A_{CP} = (\alpha_- + \alpha_+)/(\alpha_- - \alpha_+) = -0.006 \pm 0.012 \pm 0.007$, a precise direct test of charge–parity symmetry (CP) violation in Λ decays.

At the Beijing Electron–Positron Collider II (BEPC II), electrons and positrons annihilate, creating a resonance. Here, we study entangled pairs of baryons and antibaryons produced in the process $e^+e^- \to J/\psi \to \Lambda\overline{\Lambda}$, as illustrated in Fig. 1. The J/ψ resonance, a spin-1 meson with mass 3096.900(6) MeV c^{-2} and decay width 92.9(28) keV (ref. [6]), is produced at rest in a single photon annihilation process, which subsequently decays into a $\Lambda\overline{\Lambda}$ pair. The transition between the initial electron–positron pair and the final baryon–antibaryon pair includes helicity conserving and helicity-flip amplitudes[7–11]. Because the electron mass is negligible in comparison to the J/ψ mass, the initial electron and positron helicities have to be opposite. This implies that the angular distribution and polarization of the produced Λ and $\overline{\Lambda}$ particles can be described uniquely by only two quantities: the $J/\psi \to \Lambda\overline{\Lambda}$ angular distribution parameter α_ψ and the helicity phase $\Delta\Phi$. The value of the parameter α_ψ is well known[12–14], but the parameter $\Delta\Phi$ has never been measured before. If the phase difference $\Delta\Phi$ is non-vanishing, Λ and $\overline{\Lambda}$ will be polarized in the direction perpendicular to the production plane, and the magnitude of the polarization depends on the angle θ_Λ between the Λ momentum and the electron beam direction in the J/ψ rest frame (Fig. 1).

The polarization of weakly decaying particles, such as the Λ hyperons, can be inferred from the angular distribution of the daughter particles. In the case of decay $\Lambda \to p\pi^-$ and with the Λ hyperon polarization given by the vector $\mathbf{P}_\Lambda$, the angular distribution of the daughter protons is $\frac{1}{4\pi}(1 + \alpha_- \mathbf{P}_\Lambda \cdot \mathbf{n})$, where $\mathbf{n}$ is the unit vector along the proton momentum in the Λ rest frame. The asymmetry parameter α_- of the decay is bounded by $-1 \le \alpha_- \le 1$ and characterizes the degree of mixing of parity-conserving and parity-violating amplitudes in the process[15]. The corresponding asymmetry parameters α_+ for $\overline{\Lambda} \to \overline{p}\pi^+$, α_0 for $\Lambda \to n\pi^0$ and $\overline{\alpha}_0$ for $\overline{\Lambda} \to \overline{n}\pi^0$ are defined in the same way[6]. The joint angular distribution of $J/\psi \to \Lambda\overline{\Lambda}$ ($\Lambda \to f$ and $\overline{\Lambda} \to \overline{f}$, $f = p\pi^-$ or $n\pi^0$) depends on the Λ and $\overline{\Lambda}$ polarization and the spin correlation of the $\Lambda\overline{\Lambda}$ pair via the parameters α_ψ and $\Delta\Phi$. The spin correlation implies a correlation between the directions of the detected (anti-)nucleons. Together with the long lifetime of Λ and $\overline{\Lambda}$, this provides an example of a quantum entangled system as defined in refs. [16,17]. The joint angular distribution of the decay chain $J/\psi \to (\Lambda \to p\pi^-)(\overline{\Lambda} \to \overline{p}\pi^+)$ can be expressed as[4]

$$\begin{aligned}
&\mathcal{W}(\boldsymbol{\xi}; \alpha_\psi, \Delta\Phi, \alpha_-, \alpha_+) \\
&= 1 + \alpha_\psi \cos^2\theta_\Lambda + \alpha_-\alpha_+ [\sin^2\theta_\Lambda (n_{1,x}n_{2,x} - \alpha_\psi n_{1,y}n_{2,y}) \\
&+ (\cos^2\theta_\Lambda + \alpha_\psi) n_{1,z}n_{2,z}] \\
&+ \alpha_-\alpha_+ \sqrt{1-\alpha_\psi^2}\, \cos(\Delta\Phi) \sin\theta_\Lambda \cos\theta_\Lambda (n_{1,x}n_{2,z} + n_{1,z}n_{2,x}) \\
&+ \sqrt{1-\alpha_\psi^2}\, \sin(\Delta\Phi)\, \sin\theta_\Lambda \cos\theta_\Lambda (\alpha_- n_{1,y} + \alpha_+ n_{2,y})
\end{aligned} \tag{1}$$

where $\hat{\mathbf{n}}_1$ ($\hat{\mathbf{n}}_2$) is the unit vector in the direction of the nucleon (antinucleon) in the rest frame of Λ ($\overline{\Lambda}$). The components of these vectors are expressed using a coordinate system $(\hat{x}, \hat{y}, \hat{z})$ with the orientation shown in Fig. 1. The $\hat{z}$ axis of both Λ and $\overline{\Lambda}$ rest frames is oriented along the Λ momentum $\mathbf{p}_\Lambda$ in the J/ψ rest system. The $\hat{y}$ axis is perpendicular to the production plane and oriented along the vector $\mathbf{k}_- \times \mathbf{p}_\Lambda$, where $\mathbf{k}_-$ is the electron beam momentum in the J/ψ rest system. The variable ξ denotes the set of kinematic variables $(\theta_\Lambda, \hat{\mathbf{n}}_1, \hat{\mathbf{n}}_2)$, which uniquely specifies an event configuration. The terms multiplied by $\alpha_-\alpha_+$ in equation (1) represent the contribution from $\Lambda\overline{\Lambda}$ spin correlations, while the terms multiplied by α_- and α_+ separately represent the contribution from the polarization, P_y:

$$P_y(\cos\theta_\Lambda) = \frac{\sqrt{1-\alpha_\psi^2}\, \sin(\Delta\Phi) \cos\theta_\Lambda \sin\theta_\Lambda}{1 + \alpha_\psi \cos^2\theta_\Lambda} \tag{2}$$

The presence of all three contributions in equation (1) enables an unambiguous determination of the parameters α_ψ and $\Delta\Phi$ and the decay asymmetries α_-, α_+. If $\overline{\Lambda}$ is reconstructed via its $\overline{n}\pi^0$ decay, the parameters α_ψ, $\Delta\Phi$ and the decay asymmetries α_- and $\overline{\alpha}_0$ can be determined independently, because the corresponding angular distribution is obtained by replacing α_+ by $\overline{\alpha}_0$ and interpreting n_2 as the antineutron direction in equation (1). The case where Λ decays into $n\pi^0$ is not included in the present analysis because it suffers

*A full list of authors and affiliations appears in the online version of this paper.

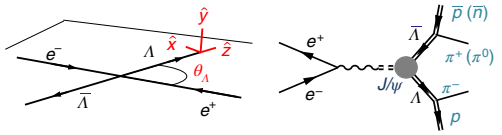

Fig. 1 | Illustration of the $e^+e^- \to J/\psi \to \Lambda\overline{\Lambda}$ process. Left: in the collision of the e^+ and e^- beams with opposite momenta the J/ψ particle is created and decays into a $\Lambda\overline{\Lambda}$ pair. The Λ particle is emitted in the $\hat{z}$ direction at an angle θ_Λ with respect to the e^- beam direction, and the $\overline{\Lambda}$ is emitted in the opposite direction. The hyperons are polarized in the direction perpendicular to the production plane ($\hat{y}$). The hyperons are reconstructed, and the polarization is determined by measuring their decay products: (anti-)nucleons and pions. Right: a Feynman diagram of $\Lambda\overline{\Lambda}$ pair production in e^+e^- annihilation with subsequent weak decays of Λ and $\overline{\Lambda}$.

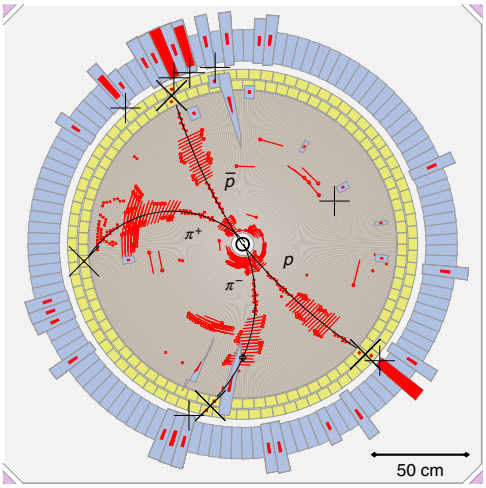

Fig. 2 | An example $J/\psi \to (\Lambda \to p\pi^-)(\overline{\Lambda} \to \overline{p}\pi^+)$ event in the BESIII detector. Cross-section of the detector in the plane perpendicular to the colliding electron–positron beams and a schematic representation of the information collected for the event. The mean decay length of the neutral $\Lambda(\overline{\Lambda})$ is 5 cm. The curved tracks of the charged particles from the subsequent $\Lambda(\overline{\Lambda})$ decays are registered in the drift chamber, indicated by the brown region of the display. The momenta of (anti-)baryons are greater than 750 MeV c^{-1} and pions are less than 300 MeV c^{-1}.

from low efficiency due to a selection criterion designed to suppress the combinatorial background.

The BESIII experiment[18] is located at the Beijing Electron–Positron Collider (BEPCII), where the centre-of-mass energy can be varied between 2 GeV and 4.6 GeV. The experiment is well known for the recent discoveries of exotic four-quark hadrons[19,20]. The cross-section of the BESIII detector in the plane perpendicular to the colliding beams is shown in Fig. 2. The inner part of the detector is a cylindrical tracking system that allows the determination of the momenta of charged particles from the track curvature in the magnetic field of a superconducting solenoid. An electromagnetic calorimeter outside the tracker measures energies deposited by particles. The signals from one $J/\psi \to (\Lambda \to p\pi^-)(\overline{\Lambda} \to \overline{p}\pi^+)$ event are shown in Fig. 2. A data sample of 1.31×10^9 J/ψ events is used in the analysis. The Λ hyperons are reconstructed using their $p\pi^-$ decays and the $\overline{\Lambda}$ hyperons using their $\overline{p}\pi^+$ or $\overline{n}\pi^0$ decays. The event reconstruction and selection procedures are described in the Methods. The resulting data samples are essentially background-free, as shown in Supplementary Figs. 1 and 2. A sample of Monte Carlo (MC) simulated events including all known J/ψ decays is used to determine the background contribution. The sizes of the final data samples are 420,593 and 47,009 events, with an estimated background of 399 ± 20 and 66.0 ± 8.2 events for the $p\pi^-\overline{p}\pi^+$ and $p\pi^-\overline{n}\pi^0$ final states, respectively. For each event the full set of the kinematic variables $\boldsymbol{\xi}$ is reconstructed.

The free parameters describing the angular distributions for the two data sets—α_ψ, $\Delta\Phi$, α_-, α_+ and $\overline{\alpha}_0$—are determined from a simultaneous unbinned maximum likelihood fit. In the fit, the likelihood function is constructed from the probability density function for an event characterized by the vector $\boldsymbol{\xi}^{(i)}$:

$$\mathcal{P}(\boldsymbol{\xi}^{(i)}; \alpha_\psi, \Delta\Phi, \alpha_-, \alpha_2) = \mathcal{C}\mathcal{W}(\boldsymbol{\xi}^{(i)}; \alpha_\psi, \Delta\Phi, \alpha_-, \alpha_2)\epsilon(\boldsymbol{\xi}^{(i)}) \quad (3)$$

with $\alpha_2 = \alpha_+$ and $\alpha_2 = \overline{\alpha}_0$ for the $p\pi^-\overline{p}\pi^+$ and $p\pi^-\overline{n}\pi^0$ data sets, respectively. The joint angular distribution $\mathcal{W}(\boldsymbol{\xi}; \alpha_\psi, \Delta\Phi, \alpha_-, \alpha_2)$ is given by equation (1), and $\epsilon(\boldsymbol{\xi})$ is the detection efficiency. The normalization factor $\mathcal{C}^{-1} = \int \mathcal{W}(\boldsymbol{\xi}; \alpha_\psi, \Delta\Phi, \alpha_-, \alpha_2)\epsilon(\boldsymbol{\xi})\mathrm{d}\boldsymbol{\xi}$ has to be evaluated for each choice of parameters (α_ψ, $\Delta\Phi$, α_-, α_2). The maximum log likelihood fit including the normalization procedure is described in the Methods. The resulting global fit describes the multidimensional angular distributions very well, as illustrated in Supplementary Figs. 3 and 4. For a crosscheck, the fit was applied to the two data sets separately, and the obtained values of the parameters agree within statistical uncertainties as shown in Supplementary Table 1. The details of the fit as well the evaluation of the systematic uncertainties are discussed in the Methods, and the contributions to the systematic uncertainty are listed in Supplementary Table 2.

A clear polarization signal, strongly dependent on the Λ direction, $\cos\theta_\Lambda$, is observed for Λ and $\overline{\Lambda}$. In Fig. 3, the moment

$$\mu(\cos\theta_\Lambda) = \frac{m}{N}\sum_{i=1}^{N_k}(n_{1,y}^{(i)} - n_{2,y}^{(i)}) \quad (4)$$

related to the polarization, is calculated for $m = 50$ bins in $\cos\theta_\Lambda$. N is the total number of events in the data sample and N_k is the number of events in the kth $\cos\theta_\Lambda$ bin. The expected angular dependence of the moment is

$$\mu(\cos\theta_\Lambda) = \frac{\alpha_- - \alpha_2}{2}\frac{1 + \alpha_\psi\cos^2\theta_\Lambda}{3 + \alpha_\psi}P_y(\theta_\Lambda) \quad (5)$$

for the acceptance corrected data. The helicity phase is determined to be $\Delta\Phi = (42.4 \pm 0.6 \pm 0.5)°$, where the first uncertainty is statistical and the second systematic. This corresponds to the Λ and $\overline{\Lambda}$ transverse polarization dependence on $\cos\theta_\Lambda$ as shown in Supplementary Fig. 5 with the maximum polarization of 24.8% (ref. [3]). This large value of $\Delta\Phi$ enables a simultaneous determination of the decay asymmetry parameters for $\Lambda \to p\pi^-$, $\overline{\Lambda} \to \overline{p}\pi^+$ and $\overline{\Lambda} \to \overline{n}\pi^0$, as shown in Table 1. The value of $\alpha_- = 0.750 \pm 0.009 \pm 0.004$ differs by more than 5 s.d. from the world average of $\alpha_-^{\mathrm{PDG}} = 0.642 \pm 0.013$ established in 1978 (PDG, Particle Data Group)[5]. We note that the two most precise results[21,22] included in the average were obtained by measuring the asymmetry in the secondary scattering of the polarized protons from Λ decays on a Carbon target. The α_- value was then determined using a compilation of the polarized proton scattering data on Carbon[23], which is no longer in use (data sets[24–26] are used instead). In addition, the average value α_-^{PDG} does not include a systematical uncertainty of 5% mentioned in ref. [21], which points to the need for a critical reevaluation of the α_-^{PDG} value. Considering the caveats concerning the current world average α_-^{PDG}, our new result implies that all published measurements on $\Lambda/\overline{\Lambda}$ polarization derived using α_-^{PDG} are $17 \pm 3\%$ too large. The value obtained for

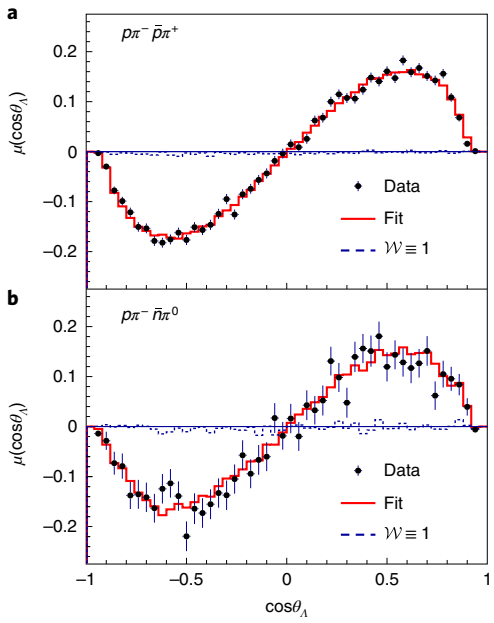

Fig. 3 | The polarization signal for $\Lambda(\overline{\Lambda})$ in $e^+e^-\to J/\psi\to\Lambda\overline{\Lambda}$. a,**b**, For each event, the weight $(n^{(i)}_{1,y}-n^{(i)}_{2,y})$ is calculated and the average weight $\mu(\cos\theta_\Lambda)$ is obtained using equation (4) for $m=50$ bins in $\cos\theta_\Lambda$. The moments $\mu(\cos\theta_\Lambda)$ are plotted as a function of $\cos\theta_\Lambda$ for $p\pi^-\bar{p}\pi^+$ (**a**) and $p\pi^-\bar{n}\pi^0$ (**b**) data sets. Filled circles indicate BESIII data and solid red lines show the result of the global fit based on equation (3). The dashed line represents the expected distribution without polarization $\mathcal{W}(\boldsymbol{\xi};0,0,0,0)\equiv 1$ in equation (3). The errors are 1 s.d. statistical and calculated by error propagation of equation (4).

Table 1 | Summary of the results

Parameters	This work	Previous results
α_ψ	$0.461\pm0.006\pm0.007$	0.469 ± 0.027 (ref. [14])
$\Delta\Phi$	$42.4\pm0.6\pm0.5°$	-
α_-	$0.750\pm0.009\pm0.004$	0.642 ± 0.013 (ref. [6])
α_+	$-0.758\pm0.010\pm0.007$	-0.71 ± 0.08 (ref. [6])
$\overline{\alpha}_0$	$-0.692\pm0.016\pm0.006$	-
A_{CP}	$-0.006\pm0.012\pm0.007$	0.006 ± 0.021 (ref. [6])
$\overline{\alpha}_0/\alpha_+$	$0.913\pm0.028\pm0.012$	-

Parameters: $J/\psi\to\Lambda\overline{\Lambda}$ angular distribution parameter α_ψ, helicity phase $\Delta\Phi$, asymmetry parameters for the $\Lambda\to p\pi^-$ (α_-), $\overline{\Lambda}\to\bar{p}\pi^+$ (α_+) and $\overline{\Lambda}\to\bar{n}\pi^0$ ($\overline{\alpha}_0$) decays, CP asymmetry A_{CP} and ratio $\overline{\alpha}_0/\alpha_+$. The first uncertainty is 1 s.d. statistical, and the second is systematic, calculated as described in the Methods.

the ratio $\overline{\alpha}_0/\alpha_+$ is 3σ smaller than unity, indicating an isospin three-half contribution to the final state[27–29]. The reported values of α_- and α_+, along with the covariance (reported in the Methods), enable a calculation of the CP odd observable $A_{CP}=(\alpha_-+\alpha_+)/(\alpha_--\alpha_+)=-0.006\pm0.012\pm0.007$, where the uncertainties refer to statistical and systematic, respectively. This is the most sensitive test of CP violation for Λ baryons with a substantially improved precision over previous measurements[30] (Table 1) using a direct method. The Standard Model calculations predict $A_{CP}\approx10^{-4}$ (ref. [31]), while larger values are expected in various extensions of the Standard Model aiming to explain the observed baryon–antibaryon asymmetry in the universe[32]. This new method to test for CP violation in baryon decays is expected to reach sensitivities comparable to theoretical predictions when larger data sets of foreseen experiments become available.

Online content

Any methods, additional references, Nature Research reporting summaries, source data, statements of code and data availability and associated accession codes are available at https://doi.org/10.1038/s41567-019-0494-8.

Received: 30 May 2018; Accepted: 11 March 2019;
Published online: 6 May 2019

References

1. Kopke, L. & Wermes, N. J/ψ decays. *Phys. Rep.* **174**, 67–227 (1989).
2. Cabibbo, N. & Gatto, R. Electron positron colliding beam experiments. *Phys. Rev.* **124**, 1577–1595 (1961).
3. Brodsky, S. J., Carlson, C. E., Hiller, J. R. & Hwang, D. S. Single spin polarization effects and the determination of time-like proton form-factors. *Phys. Rev. D* **69**, 054022 (2004).
4. Fäldt, G. & Kupsc, A. Hadronic structure functions in the $e^+e^-\to\overline{\Lambda}\Lambda$ reaction. *Phys. Lett. B* **772**, 16–20 (2017).
5. Bricman, C. et al. Review of particle properties. *Phys. Lett. B* **75**, 1–250 (1978).
6. Tanabashi, M. et al. Review of particle physics. *Phys. Rev. D* **98**, 030001 (2018).
7. Dubnickova, A. Z., Dubnicka, S. & Rekalo, M. P. Investigation of the nucleon electromagnetic structure by polarization effects in $e^+e^-\to N\overline{N}$ processes. *Nuovo Cim. A* **109**, 241–256 (1996).
8. Gakh, G. I. & Tomasi-Gustafsson, E. General analysis of polarization phenomena in $e^++e^-\to N+\overline{N}$ for axial parametrization of two-photon exchange. *Nucl. Phys. A* **771**, 169–183 (2006).
9. Czyz, H., Grzelinska, A. & Kuhn, J. H. Spin asymmetries and correlations in lambda-pair production through the radiative return method. *Phys. Rev. D* **75**, 074026 (2007).
10. Fäldt, G. Entanglement in joint $\Lambda\overline{\Lambda}$ decay. *Eur. Phys. J. A* **51**, 74 (2015).
11. Fäldt, G. Polarization observables in the $e^+e^-\to\overline{\Lambda}\Lambda$ reaction. *Eur. Phys. J. A* **52**, 141 (2016).
12. Bai, J. Z. et al. Decays of the J/ψ to $\Lambda\overline{\Lambda}$, $\Lambda\overline{\Lambda}\gamma$ and $\Lambda\overline{\Lambda}$, $\Lambda\overline{\Lambda}\gamma$ final states. *Phys. Lett. B* **424**, 213–218 (1998). Erratum **438**, 447 (1998).
13. Ablikim, M. et al. Measurement of J/ψ decays into $\Lambda\overline{\Lambda}\pi^+\pi^-$. *Chin. Phys. C* **36**, 1031–1039 (2012).
14. Ablikim, M. et al. Study of J/ψ and $\psi(3686)$ decay to $\Lambda\overline{\Lambda}$ and $\Lambda\overline{\Lambda}$ final states. *Phys. Rev. D* **95**, 052003 (2017).
15. Lee, T. D. & Yang, C.-N. General partial wave analysis of the decay of a hyperon of spin 1/2. *Phys. Rev.* **108**, 1645–1647 (1957).
16. Tornqvist, N. A. Suggestion for Einstein–Podolsky–Rosen experiments using reactions like $e^+e^-\to\Lambda\overline{\Lambda}\to\pi^-p\pi^+\overline{p}$. *Found. Phys.* **11**, 171–177 (1981).
17. Hiesmayr, B. C. Limits of quantum information in weak interaction processes of hyperons. *Sci. Rep.* **5**, 11591 (2015).
18. Ablikim, M. et al. Design and construction of the BESIII detector. *Nucl. Instrum. Methods* **A614**, 345–399 (2010).
19. Ablikim, M. et al. Observation of a charged charmonium like structure in $e^+e^-\to\pi^+\pi^-J/\psi$ at $\sqrt{s}=4.26$ GeV. *Phys. Rev. Lett.* **110**, 252001 (2013).
20. Shepherd, M. R., Dudek, J. J. & Mitchell, R. E. Searching for the rules that govern hadron construction. *Nature* **534**, 487–493 (2016).
21. Overseth, O. E. & Roth, R. F. Time reversal invariance in Λ^0 decay. *Phys. Rev. Lett.* **19**, 391–393 (1967).
22. Cleland, W. E. et al. A measurement of the beta-parameter in the charged nonleptonic decay of the Λ^0 hyperon. *Nucl. Phys.* **B40**, 221–254 (1972).
23. Peterson, V. Z. *Analyzing Power of Carbon for High-Energy Polarized Protons* Report No. LRL-UCRL-10622 https://escholarship.org/uc/item/7777n2h0 (1963).
24. Besset, D. et al. Proton Carbon analyzing power between 300 MeV and 560 MeV. *Nucl. Instrum. Methods* **166**, 379–389 (1979).
25. Aprile-Giboni, E. et al. Proton carbon effective analyzing power between 95 MeV and 570 MeV. *Nucl. Instrum. Methods* **215**, 147–157 (1983).
26. Mcnaughton, M. W. et al. The p-C analyzing power between 100 MeV and 750 MeV. *Nucl. Instrum. Methods* **A241**, 435–440 (1985).
27. Overseth, O. E. & Pakvasa, S. Final-state interactions in nonleptonic hyperon decay. *Phys. Rev.* **184**, 1663–1667 (1969).
28. Olsen, S. et al. Asymmetry parameter for $\Lambda^0\to n\pi^0$. *Phys. Rev. Lett.* **24**, 843–847 (1970).
29. Cheng, H.-Y. Status of the $\Delta I=1/2$ rule in kaon decay. *Int. J. Mod. Phys.* **A4**, 495 (1989).
30. Barnes, P. D. et al. Observables in high statistics measurements of the reaction $\overline{p}p\to\overline{\Lambda}\Lambda$. *Phys. Rev. C* **54**, 1877–1886 (1996).

31. Donoghue, J. F., He, X.-G. & Pakvasa, S. Hyperon decays and CP nonconservation. *Phys. Rev. D* **34**, 833–842 (1986).
32. Bigi, I. I., Kang, X.-W. & Li, H.-B. CP asymmetries in strange baryon decays. *Chin. Phys. C* **42**, 013101 (2018).

Acknowledgements

The BESIII collaboration thanks the staff of BEPCII and the IHEP computing centre for their support. This work is supported in part by the National Key Basic Research Program of China under contract no. 2015CB856700; the National Natural Science Foundation of China (NSFC) under contract nos. 11335008, 11375205, 11425524, 11625523, 11635010, 11735014, 11835012 and 11875054; the Chinese Academy of Sciences (CAS) Large-Scale Scientific Facility Program; the CAS Center for Excellence in Particle Physics (CCEPP); Joint Large-Scale Scientific Facility Funds of the NSFC and CAS under contract nos. U1532257, U1532258, U1732102, U1732263 and U1832207; CAS Key Research Program of Frontier Sciences under contract nos. QYZDJ-SSW-SLH003 and QYZDJ-SSW-SLH040; 100 Talents Program of CAS; the CAS President's International Fellowship Initiative; INPAC and Shanghai Key Laboratory for Particle Physics and Cosmology; German Research Foundation DFG under the contracts Collaborative Research Center CRC 1044 and FOR 2359; Istituto Nazionale di Fisica Nucleare, Italy; Koninklijke Nederlandse Akademie van Wetenschappen (KNAW) under contract no. 530-4CDP03; Ministry of Development of Turkey under contract no. DPT2006K-120470; National Science and Technology fund; The Swedish Research Council; the Knut and Alice Wallenberg Foundation; US Department of Energy under contract nos. DE-FG02-05ER41374, DE-SC-0010118, DE-SC-0010504 and DE-SC-0012069; University of Groningen (RuG); Helmholtzzentrum fuer Schwerionenforschung GmbH (GSI), Darmstadt. All consortium work was carried out at affiliations 1–67.

Author contributions

All authors have contributed to this publication, being variously involved in the design and construction of the detectors, writing software, calibrating sub-systems, operating the detectors, acquiring data and analysing the processed data.

Competing interests

The authors declare no competing interests.

Additional information

Supplementary information is available for this paper at https://doi.org/10.1038/s41567-019-0494-8.

Reprints and permissions information is available at www.nature.com/reprints.

Correspondence and requests for materials should be addressed to A.Kupsc.

Journal peer review information: *Nature Physics* thanks Anna Zuzana Dubnickova, Ulrik Egede and Ilya Selyuzhenkov for their contribution to the peer review of this work.

Publisher's note: Springer Nature remains neutral with regard to jurisdictional claims in published maps and institutional affiliations.

Methods

Monte Carlo simulation. The optimization of event selection criteria and the estimation of backgrounds are based on Monte Carlo (MC) simulations. The Geant4-based simulation software includes the geometry and the material description of the BESIII spectrometer, the detector response and the digitization models, as well as the database of the running conditions and detector performance. Production of the J/ψ resonance is simulated by the MC event generator kkmc[33]; the known decays are generated by Besevtgen[34,35] with branching ratios set to the world average values[6], and missing decays are generated by the Lundcharm[36] model with optimized parameters[37]. Signal and background events are generated using helicity amplitudes. For the signal process $J/\psi\to\Lambda\overline{\Lambda}$, the angular distribution of equation (1) is used. For the backgrounds, $J/\psi\to\Sigma^0\overline{\Sigma}^0$, $\Sigma^+\overline{\Sigma}^-$ and $\Lambda\overline{\Sigma}^0+$c.c. decays, the helicity amplitudes are taken from ref. [38] and the angular distribution parameters are fixed to −0.24 (ref. [39]) for $J/\psi\to\Sigma^0\overline{\Sigma}^0$ and $J/\psi\to\Sigma^+\overline{\Sigma}^-$ and to 0.38 (ref. [40]) for $J/\psi\to\Lambda\overline{\Sigma}^0+$c.c.

General selection criteria. Charged tracks detected in the main drift chamber (MDC) must satisfy $|\cos\theta|<0.93$, where θ is the polar angle with respect to the positron beam direction. No additional particle identification requirements are applied to select the tracks. Showers in the electromagnetic calorimeter (EMC) not associated with any charged track are identified as photon candidates if they fulfil the following requirements: the deposited energy is required to be larger than 25 MeV and 50 MeV for clusters reconstructed in the barrel ($|\cos\theta|<0.8$) and end cap ($0.86<|\cos\theta|<0.92$), respectively. To suppress electronic noise and showers unrelated to the event, the EMC time difference from the event start time is required to be within [0, 700] ns. To remove showers originating from charged particles, the angle between the shower position and charged tracks extrapolated to the EMC must be greater than 10°.

Selection of $J/\psi\to\Lambda\overline{\Lambda}$, $\Lambda\to p\pi^-$, $\overline{\Lambda}\to\bar{p}\pi^+$. Events with at least four charged tracks are selected. Fits of the Λ and $\overline{\Lambda}$ vertices are performed using all pairs of positive and negative charged tracks. There should be at least one $\Lambda\overline{\Lambda}$ pair in an event. If more than one set of $\Lambda\overline{\Lambda}$ pairs is found (the fraction of such events is 1.18%), the one with the smallest value of $(M_{p\pi^-}-M_\Lambda)^2+(M_{\bar{p}\pi^+}-M_\Lambda)^2$, where M_Λ is the nominal Λ mass, is retained for further analysis. A four-constraint kinematic fit imposing overall energy–momentum conservation (4C-fit) is performed with the $\Lambda\to p\pi^-$ and $\overline{\Lambda}\to\bar{p}\pi^+$ hypothesis, and events with $\chi^2<60$ are retained. The invariant masses of $p\pi^-$ and $\bar{p}\pi^+$ are required to be within $|M_{p\pi^-}-M_\Lambda|<5\,\mathrm{MeV}\,c^{-2}$ and $|M_{\bar{p}\pi^+}-M_\Lambda|<5\,\mathrm{MeV}\,c^{-2}$. The $p\pi^-$ and $\bar{p}\pi^+$ invariant mass spectra and the selection windows are shown in Supplementary Fig. 1.

Selection of $J/\psi\to\Lambda\overline{\Lambda}$, $\Lambda\to p\pi^-$, $\overline{\Lambda}\to\bar{n}\pi^0$. Events with at least two charged tracks and at least three showers are selected. Two showers, consistent with being photons, are used to reconstruct the π^0 candidates, and the invariant mass of the photon pair is required to be in the interval [0.12, 0.15] GeV c^{-2}. To improve the momentum resolution, a mass-constrained fit to the π^0 nominal mass is applied to the photon pairs, and the resulting energy and momentum of the π^0 are used for further analysis. Candidates for Λ are formed by combining two oppositely charged tracks into the final states $p\pi^-$. The two daughter tracks are constrained to originate from a common decay vertex by requiring the χ^2 of the vertex fit to be less than 100. The maximum energy for the photons from π^0 decays in these events is 300 MeV. Therefore, showers produced by $\bar{n}$ can be uniquely identified by selecting the cluster with an energy deposit larger than 350 MeV. In addition, the second moment of the cluster is required to be larger than 20 cm^2. The moment is defined as $\sum_i E_i r_i^2/\sum_i E_i$, where E_i is the deposited energy in the ith crystal, and r_i is the radial distance of the crystal i from the cluster centre. To select the $J/\psi\to\Lambda(p\pi^-)\overline{\Lambda}(\bar{n}\pi^0)$ candidate events, a one-constraint (1C) kinematic fit is performed, where the momentum of the anti-neutron is unmeasured. The selected events are required to have a $\chi^2_{1C-\bar{n}}$ of the 1C kinematic fit less than 10, and if there is more than one combination, the one with the smallest $\chi^2_{1C-\bar{n}}$ value is chosen. To further suppress background contributions, we require $|M_{p\pi^-}-M_\Lambda|<5\,\mathrm{MeV}\,c^{-2}$, where M_Λ is the nominal Λ mass. Supplementary Fig. 2 shows the invariant mass $(M_{\bar{n}\pi^0})$ of the $\bar{n}\pi^0$ pair and the mass $M^{\mathrm{Recoiling}}_{\Lambda\pi^0}$ recoiling against the $\Lambda\pi^0$, where $M_{\bar{n}\pi^0}=\sqrt{(E_{\bar{n}}+E_{\pi^0})^2-(\vec{P}_{\bar{n}}+\vec{P}_{\pi^0})^2}$, $\vec{P}_{\bar{n}}=-(\vec{P}_\Lambda+\vec{P}_{\pi^0})$ is evaluated in the rest frame of J/ψ, and $E_{\bar{n}}=\sqrt{|\vec{P}_{\bar{n}}|^2+M_n^2}$ (with M_n the nominal neutron mass). The signal regions are defined as $|M_{\bar{n}\pi^0}-M_\Lambda|<23\,\mathrm{MeV}\,c^{-2}$ and $|M^{\mathrm{Recoiling}}_{\Lambda\pi^0}-M_n|<7\,\mathrm{MeV}\,c^{-2}$ as shown in Supplementary Fig. 2. The above selection strategy is not suitable for the channel $J/\psi\to\Lambda\overline{\Lambda}$, $\Lambda\to n\pi^0$, $\overline{\Lambda}\to\bar{p}\pi^+$. The reason for this is the requirement of the energy deposit of 350 MeV used to identify the neutron cluster. We estimate that the overall efficiency would be lower by at least a factor of four with respect to the $J/\psi\to\Lambda\overline{\Lambda}$, $\Lambda\to p\pi^-$, $\overline{\Lambda}\to\bar{n}\pi^0$ channel.

Background analysis. The potential backgrounds are studied using the inclusive MC sample for J/ψ decays. After applying the same selection criteria as for the signal, the main backgrounds for the $\overline{\Lambda}\to\bar{p}\pi^+$ final state are from $J/\psi\to\gamma\Lambda\overline{\Lambda}$, $\Lambda\overline{\Sigma}^0+$c.c., $\Sigma^0\overline{\Sigma}^0$, $\Delta^{++}\bar{p}\pi^-+$c.c., $\Delta^{++}\overline{\Delta}^{--}$ and $p\pi^-\bar{p}\pi^+$ decays. Decays of $J/\psi\to\Lambda\overline{\Sigma}^0+$c.c. and $\Sigma^0\overline{\Sigma}^0$ are generated using the helicity amplitudes and include subsequent Λ and $\overline{\Lambda}$ decays. The remaining decay modes are generated according to the phase space model, and the contribution is shown in Supplementary Fig. 1. For the $\overline{\Lambda}\to\bar{n}\pi^0$ final state, the dominant background processes are from the decay modes $J/\psi\to\gamma\Lambda\overline{\Lambda}$, $\Lambda\overline{\Sigma}^0+$c.c., $\Sigma^0(\gamma\Lambda)\overline{\Sigma}^0(\gamma\overline{\Lambda})$, $\Sigma^+(p\pi^0)\overline{\Sigma}^-(\bar{n}\pi^-)$ and $\Lambda(p\pi^-)\overline{\Lambda}(\bar{p}\pi^+)$. Exclusive MC samples for these background channels are generated and used to estimate the background contamination shown in Supplementary Fig. 2.

The global fit. Based on the joint angular distribution shown in equation (1), a simultaneous fit is performed to the two data sets according to the decay modes:

$$\mathrm{I}: J/\psi\to\Lambda\overline{\Lambda},\Lambda\to p\pi^-\ \text{and}\ \overline{\Lambda}\to\bar{p}\pi^+$$
$$\mathrm{II}: J/\psi\to\Lambda\overline{\Lambda},\Lambda\to p\pi^-\ \text{and}\ \overline{\Lambda}\to\bar{n}\pi^0$$

There are three common parameters (α_ψ, $\Delta\Phi$ and α_-) and two separate parameters (α_+ and $\bar{\alpha}_0$) for the $\overline{\Lambda}$ decays to $\bar{p}\pi^+$ and $\bar{n}\pi^0$, respectively. For data set I, the joint likelihood function is defined as[38]

$$\begin{aligned}\mathcal{L}^{\mathrm{I}} &= \prod_{i=1}^{N^{\mathrm{I}}}\mathcal{P}(\xi_{\mathrm{I}}^{(i)};\alpha_\psi,\Delta\Phi,\alpha_-,\alpha_+)\\ &= (\mathcal{C}^{\mathrm{I}})^{N^{\mathrm{I}}}\prod_{i=1}^{N^{\mathrm{I}}}\mathcal{W}(\xi_{\mathrm{I}}^{(i)};\alpha_\psi,\Delta\Phi,\alpha_-,\alpha_+)\epsilon(\xi_{\mathrm{I}}^{(i)})\end{aligned}\tag{6}$$

where $\mathcal{P}(\xi_{\mathrm{I}}^{(i)};\alpha_\psi,\Delta\Phi,\alpha_-,\alpha_+)$ is the probability density function defined in equation (3) and evaluated for the kinematic variables $\xi_{\mathrm{I}}^{(i)}$ of event i, and $\mathcal{W}(\xi_{\mathrm{I}}^{(i)};\alpha_\psi,\Delta\Phi,\alpha_-,\alpha_+)$ is defined in equation (1). The detection efficiency terms, $\epsilon(\xi_{\mathrm{I}}^{(i)})$, can be set arbitrarily to one because they do not influence the minimization of the function $-\ln\mathcal{L}^{\mathrm{I}}$ with respect to the parameters α_ψ, $\Delta\Phi$, α_- and α_+. The normalization factor $(\mathcal{C}^{\mathrm{I}})^{-1}=\frac{1}{N_{\mathrm{MC}}}\sum_{j=1}^{N_{\mathrm{MC}}}\mathcal{W}(\xi^{(j)}I;\alpha_\psi,\Delta\Phi,\alpha_-,\alpha_+)$ is estimated with the accepted N_{MC} events, which are generated with the phase space model, undergo detector simulation and are selected with the same event criteria as for data. To ensure an accurate value for the normalization factor, N_{MC} is 7,850,525 for $p\bar{p}\pi^+\pi^-$ and 907,253 for $p\bar{n}\pi^+\pi^0$. The definition of the likelihood function for data set II, $\mathcal{L}^{\mathrm{II}}$, is the same except for its calculation with different parameters and data set. To determine the parameters, we use the package MINUIT from the CERN library[41] to minimize the function defined as

$$S=-\ln\mathcal{L}^{\mathrm{I}}_{\mathrm{data}}-\ln\mathcal{L}^{\mathrm{II}}_{\mathrm{data}}+\ln\mathcal{L}^{\mathrm{I}}_{\mathrm{bg.}}+\ln\mathcal{L}^{\mathrm{II}}_{\mathrm{bg.}}\tag{7}$$

where $\ln\mathcal{L}^{\mathrm{I(II)}}_{\mathrm{data}}$ and $\ln\mathcal{L}^{\mathrm{I(II)}}_{\mathrm{bg.}}$ are the likelihood functions for the two data sets and the background events taken from simulation, respectively. The results of the separate fits for the two data sets are given in Supplementary Table 1. We compare the fit with the data using moments $T_1,\ldots,T_5$ directly related to the terms in equation (1). The moments are calculated for 100 bins in $\cos\theta_\Lambda$ and are explicitly given by

$$\begin{aligned}T_1&=\sum_{i=1}^{N_k}(\sin^2\theta_\Lambda n^{(i)}_{1,x}n^{(i)}_{2,x}+\cos^2\theta_\Lambda n^{(i)}_{1,z}n^{(i)}_{2,z})\\ T_2&=-\sum_{i=1}^{N_k}\sin\theta_\Lambda\cos\theta_\Lambda(n^{(i)}_{1,x}n^{(i)}_{2,z}+n^{(i)}_{1,z}n^{(i)}_{2,x})\\ T_3&=-\sum_{i=1}^{N_k}\sin\theta_\Lambda\cos\theta_\Lambda n^{(i)}_{1,y}\\ T_4&=-\sum_{i=1}^{N_k}\sin\theta_\Lambda\cos\theta_\Lambda n^{(i)}_{2,y}\\ T_5&=\sum_{i=1}^{N_k}(n^{(i)}_{1,z}n^{(i)}_{2,z}-\sin^2\theta_\Lambda n^{(i)}_{1,y}n^{(i)}_{2,y})\end{aligned}\tag{8}$$

where N_k is the number of events in the kth $\cos\theta_\Lambda$ bin. Supplementary Figs. 3 and 4 show the moments and the Λ angular distribution for data compared to those calculated using the probability density function $\mathcal{P}(\boldsymbol{\xi};\alpha_\psi,\Delta\Phi,\alpha_-,\alpha_2)$ with the parameters set to the values from the global fit. The unsymmetric distributions of T_3 and T_4 indicate that significant transverse polarization of Λ and $\overline{\Lambda}$ hyperons is observed. The simultaneous fit results for α_ψ, α_-, α_+, $\Delta\Phi$ and $\bar{\alpha}_0$ parameters are given in Supplementary Table 1. Based on these parameters, the observables $\bar{\alpha}_0/\alpha_+$ and $A_{\mathrm{CP}}=(\alpha_-+\alpha_+)/(\alpha_--\alpha_+)$ are calculated, and their statistical uncertainties are evaluated taking into account the correlation coefficients $\rho(\alpha_+,\alpha_0)=0.42$ and $\rho(\alpha_+,\alpha_-)=0.82$, respectively. As a cross-check, separate fits to data sets I and II are performed, and the results are consistent with the simultaneous fit within statistical uncertainties, as shown in Supplementary Table 1.

Systematic uncertainty. The systematic uncertainties can be divided into two categories. The first category is from the event selection, including the uncertainties on MDC tracking efficiency, the kinematic fit, π^0 and $\bar{n}$ efficiencies,

Λ and $\bar{\Lambda}$ reconstruction, background estimation and the Λ, $\bar{\Lambda}$ and $M_{\Lambda\pi^0}^{\mathrm{Recoiling}}$ mass window requirements. The second category includes uncertainties associated with the fit procedure based on equations (1) and (3).

(1) The uncertainty due to the efficiency of charged particle tracking has been investigated with control samples of $J/\psi \to \Lambda\bar{\Lambda} \to p\pi^-\bar{p}\pi^+$ (ref. [42]), taking into consideration the correlation between the magnitude of charged particle momentum and its polar angle acceptances. Corrections are made based on the two-dimensional distribution of track momentum versus polar angle. The difference between the fit results with and without the tracking correction is taken as a systematic uncertainty.

(2) The uncertainty due to the π^0 reconstruction is estimated from the difference between data and MC simulation using a $J/\psi \to \pi^+\pi^-\pi^0$ control sample. The uncertainty due to the $\bar{n}$ shower requirement is estimated with a $J/\psi \to p\pi^-\bar{n}$ control sample, and the correction factors between data and MC simulations are determined. The differences in the fit results with and without corrections to the efficiencies of the π^0 and $\bar{n}$ reconstructions are taken as systematic uncertainties.

(3) The systematic uncertainties for the determination of the physics parameters in the fits due to the Λ and $\bar{\Lambda}$ vertex reconstructions are found to be negligible.

(4) The systematic uncertainties due to kinematic fits are determined by making corrections to the track parameters distributions in the MC simulations to better match the data. The corrections are done with the five-dimensional distributions over the θ_Λ, $\hat{\mathbf{n}}_1$, $\hat{\mathbf{n}}_2$ variables, where $\hat{\mathbf{n}}_1$ and $\hat{\mathbf{n}}_2$ are expressed using spherical coordinates. The fit to data with the corrected MC sample yields $\alpha_\psi = 0.462 \pm 0.006$, $\alpha_- = 0.749 \pm 0.009$, $\alpha_+ = -0.752 \pm 0.009$ and $\bar{\alpha}_0 = -0.688 \pm 0.017$. The differences between the fit with corrections and the nominal fit are considered as the systematic uncertainties. For α_ψ, the difference between the fit results with and without this correction is negligible.

(5) A possible bias and uncertainty due to the fit procedure is estimated using MC simulation, where the parameters in the joint angular distribution equation (1) are set to the central values of Table 1 and the number of generated events is the same as for the data. This procedure tests also if the number of MC events used for normalization of the probability density function in equation (6) is sufficient.

(6) The systematic uncertainty caused by the background estimation is studied by fitting the data with and without considering background subtraction. The differences in the parameters are taken as the systematic uncertainties. The contamination rate of background events in this analysis is less than 0.1% according to the full MC simulations, and the uncertainty due to the background estimation is negligible.

The total systematic uncertainty for the parameters is obtained by summing the individual systematic uncertainties in quadrature (summarized in Supplementary Table 2).

Data availability

The data that support the plots within this paper and other findings of this study are available from the corresponding author upon reasonable request.

References

33. Jadach, S., Ward, B. F. L. & Was, Z. The precision Monte Carlo event generator *KK* for two fermion final states in e^+e^- collisions. *Comput. Phys. Commun.* **130**, 260–325 (2000).
34. Lange, D. J. The EvtGen particle decay simulation package. *Nucl. Instrum. Methods* **A462**, 152–155 (2001).
35. Ping, R.-G. Event generators at BESIII. *Chin. Phys. C* **32**, 599 (2008).
36. Chen, J. C., Huang, G. S., Qi, X. R., Zhang, D. H. & Zhu, Y. S. Event generator for J/ψ and $\psi(2S)$ decay. *Phys. Rev. D* **62**, 034003 (2000).
37. Yang, R.-L., Ping, R.-G. & Chen, H. Tuning and validation of the Lundcharm model with J/ψ decays. *Chin. Phys. Lett.* **31**, 061301 (2014).
38. Zhong, B., Ping, R.-G. & Xiao, Z.-J. Study of $\bar{\Lambda}$ decay parameter in $\bar{\Lambda}$ decay. *Chin. Phys. C* **32**, 692 (2008).
39. Ablikim, M. et al. Study of J/ψ decays to $\Lambda\bar{\Lambda}$ and $\Lambda\bar{\Lambda}$. *Phys. Lett. B* **632**, 181–186 (2006).
40. Ablikim, M. et al. First observation of the isospin violating decay $J/\psi \to \Lambda\bar{\Sigma}^0 + c.c.$ *Phys. Rev. D* **86**, 032008 (2012).
41. James, F. & Roos, M. Minuit: a system for function minimization and analysis of the parameter errors and correlations. *Comput. Phys. Commun.* **10**, 343–367 (1975).
42. Ablikim, M. et al. Amplitude analysis of the $D^+ \to K_S^0\pi^+\pi^0$ Dalitz plot. *Phys. Rev. D* **89**, 052001 (2014).

The BESIII Collaboration

M. Ablikim[1], M. N. Achasov[2,68], S. Ahmed[3], M. Albrecht[4], M. Alekseev[5,6], A. Amoroso[5,6], F. F. An[1], Q. An[7,8], Y. Bai[9], O. Bakina[10], R. Baldini Ferroli[11], Y. Ban[12], K. Begzsuren[13], D. W. Bennett[14], J. V. Bennett[15], N. Berger[16], M. Bertani[11], D. Bettoni[17], F. Bianchi[5,6], E. Boger[10,69], I. Boyko[10], R. A. Briere[15], H. Cai[18], X. Cai[1,7], A. Calcaterra[11], G. F. Cao[1,19], S. A. Cetin[20,21,22], J. Chai[6], J. F. Chang[1,7], W. L. Chang[1,19], G. Chelkov[10,69,70], G. Chen[1], H. S. Chen[1,19], J. C. Chen[1], M. L. Chen[1,7], P. L. Chen[23], S. J. Chen[24], X. R. Chen[25], Y. B. Chen[1,7], W. Cheng[6], X. K. Chu[12], G. Cibinetto[17], F. Cossio[6], H. L. Dai[1,7], J. P. Dai[26,71], A. Dbeyssi[3], D. Dedovich[10], Z. Y. Deng[1], A. Denig[16], I. Denysenko[10], M. Destefanis[5,6], F. De Mori[5,6], Y. Ding[27], C. Dong[28], J. Dong[1,7], L. Y. Dong[1,19], M. Y. Dong[1,7,19], Z. L. Dou[24], S. X. Du[29], P. F. Duan[1], J. Z. Fan[30], J. Fang[1,7], S. S. Fang[1,19], Y. Fang[1], R. Farinelli[17,31], L. Fava[6,32], S. Fegan[16], F. Feldbauer[4], G. Felici[11], C. Q. Feng[7,8], E. Fioravanti[17], M. Fritsch[4], C. D. Fu[1], Q. Gao[1], X. L. Gao[7,8], Y. Gao[30], Y. G. Gao[33], Z. Gao[7,8], B. Garillon[16], I. Garzia[17], A. Gilman[34], K. Goetzen[35], L. Gong[28], W. X. Gong[1,7], W. Gradl[16], M. Greco[5,6], L. M. Gu[24], M. H. Gu[1,7], Y. T. Gu[36], A. Q. Guo[1], L. B. Guo[37], R. P. Guo[1,19], Y. P. Guo[16], A. Guskov[10], Z. Haddadi[38], S. Han[18], X. Q. Hao[39], F. A. Harris[40], K. L. He[1,19], F. H. Heinsius[4], T. Held[4], Y. K. Heng[1,7,19], Z. L. Hou[1], H. M. Hu[1,19], J. F. Hu[26,71], T. Hu[1,7,19], Y. Hu[1], G. S. Huang[7,8], J. S. Huang[39], X. T. Huang[41], X. Z. Huang[24], Z. L. Huang[27], T. Hussain[42], W. Ikegami Andersson[43], M. Irshad[7,8], Q. Ji[1], Q. P. Ji[39], X. B. Ji[1,19], X. L. Ji[1,7], H. L. Jiang[41], X. S. Jiang[1,7,19], X. Y. Jiang[28], J. B. Jiao[41], Z. Jiao[44], D. P. Jin[1,7,19], S. Jin[24], Y. Jin[45], T. Johansson[43], A. Julin[34], N. Kalantar-Nayestanaki[38], X. S. Kang[28], M. Kavatsyuk[38], B. C. Ke[1], I. K. Keshk[4], T. Khan[7,8], A. Khoukaz[46], P. Kiese[16], R. Kiuchi[1], R. Kliemt[35], L. Koch[47], O. B. Kolcu[21,72], B. Kopf[4], M. Kornicer[40], M. Kuemmel[4], M. Kuessner[4], A. Kupsc[43*], M. Kurth[1], W. Kühn[47], J. S. Lange[47],

P. Larin[3], L. Lavezzi[6], S. Leiber[4], H. Leithoff[16], C. Li[43], Cheng Li[7,8], D. M. Li[29], F. Li[1,7], F. Y. Li[12], G. Li[1], H. B. Li[1,19], H. J. Li[1,19], J. C. Li[1], J. W. Li[48], K. J. Li[49], Kang Li[50], Ke Li[1], Lei Li[51], P. L. Li[7,8], P. R. Li[19,52], Q. Y. Li[41], T. Li[41], W. D. Li[1,19], W. G. Li[1], X. L. Li[41], X. N. Li[1,7], X. Q. Li[28], Z. B. Li[49], H. Liang[7,8], Y. F. Liang[53], Y. T. Liang[47], G. R. Liao[54], L. Z. Liao[1,19], J. Libby[55], C. X. Lin[49], D. X. Lin[3], B. Liu[26,71], B. J. Liu[1], C. X. Liu[1], D. Liu[7,8], D. Y. Liu[26,71], F. H. Liu[56], Fang Liu[1], Feng Liu[33], H. B. Liu[36], H. L Liu[9], H. M. Liu[1,19], Huanhuan Liu[1], Huihui Liu[57], J. Liu[1], J. B. Liu[7,8], J. Y. Liu[1,19], K. Y. Liu[27], Ke Liu[33], L. D. Liu[12], Q. Liu[19], S. B. Liu[7,8], X. Liu[25], Y. B. Liu[28], Z. A. Liu[1,7,19], Zhiqing Liu[16], Y. F. Long[12], X. C. Lou[1,7,19], H. J. Lu[44], J. G. Lu[1,7], Y. Lu[1], Y. P. Lu[1,7], C. L. Luo[37], M. X. Luo[58], P. W. Luo[49], T. Luo[59,73], X. L. Luo[1,7], S. Lusso[6], X. R. Lyu[19], F. C. Ma[27], H. L. Ma[1], L. L. Ma[41], M. M. Ma[1,19], Q. M. Ma[1], X. N. Ma[28], X. Y. Ma[1,7], X. X. Ma[1,19], Y. M. Ma[41], F. E. Maas[3], M. Maggiora[5,6], S. Maldaner[16], Q. A. Malik[42], A. Mangoni[60], Y. J. Mao[12], Z. P. Mao[1], S. Marcello[5,6], Z. X. Meng[45], J. G. Messchendorp[38], G. Mezzadri[17], J. Min[1,7], T. J. Min[24], R. E. Mitchell[14], X. H. Mo[1,7,19], Y. J. Mo[33], C. Morales Morales[3], N. Yu. Muchnoi[2,68], H. Muramatsu[34], A. Mustafa[4], S. Nakhoul[35,74], Y. Nefedov[10], F. Nerling[35,74], I. B. Nikolaev[2,68], Z. Ning[1,7], S. Nisar[61], S. L. Niu[1,7], X. Y. Niu[1,19], S. L. Olsen[19], Q. Ouyang[1,7,19], S. Pacetti[60], Y. Pan[7,8], M. Papenbrock[43], P. Patteri[11], M. Pelizaeus[4], J. Pellegrino[5,6], H. P. Peng[7,8], Z. Y. Peng[36], K. Peters[35,74], J. Pettersson[43], J. L. Ping[37], R. G. Ping[1,19], A. Pitka[4], R. Poling[34], V. Prasad[7,8], H. R. Qi[62], M. Qi[24], T. Y. Qi[62], S. Qian[1,7], C. F. Qiao[19], N. Qin[18], X. S. Qin[4], Z. H. Qin[1,7], J. F. Qiu[1], S. Q. Qu[28], K. H. Rashid[42,75], C. F. Redmer[16], M. Richter[4], M. Ripka[16], A. Rivetti[6], M. Rolo[6], G. Rong[1,19], Ch. Rosner[3], M. Rump[46], A. Sarantsev[10,76], M. Savrié[31], K. Schoenning[43], W. Shan[63], X. Y. Shan[7,8], M. Shao[7,8], C. P. Shen[62], P. X. Shen[28], X. Y. Shen[1,19], H. Y. Sheng[1], X. Shi[1,7], J. J. Song[41], W. M. Song[41], X. Y. Song[1], S. Sosio[5,6], C. Sowa[4], S. Spataro[5,6], F. F. Sui[41], G. X. Sun[1], J. F. Sun[39], L. Sun[18], S. S. Sun[1,19], X. H. Sun[1], Y. J. Sun[7,8], Y. K Sun[7,8], Y. Z. Sun[1], Z. J. Sun[1,7], Z. T. Sun[1], Y. T Tan[7,8], C. J. Tang[53], G. Y. Tang[1], X. Tang[1], M. Tiemens[38], B. Tsednee[13], I. Uman[64], B. Wang[1], B. L. Wang[19], C. W. Wang[24], D. Wang[12], D. Y. Wang[12], Dan Wang[19], H. H. Wang[41], K. Wang[1,7], L. L. Wang[1], L. S. Wang[1], M. Wang[41], Meng Wang[1,19], P. Wang[1], P. L. Wang[1], W. P. Wang[7,8], X. F. Wang[1], Y. Wang[7,8], Y. F. Wang[1,7,19], Z. Wang[1,7], Z. G. Wang[1,7], Z. Y. Wang[1], Zongyuan Wang[1,19], T. Weber[4], D. H. Wei[54], P. Weidenkaff[16], S. P. Wen[1], U. Wiedner[4], M. Wolke[43], L. H. Wu[1], L. J. Wu[1,19], Z. Wu[1,7], L. Xia[7,8], X. Xia[41], Y. Xia[65], D. Xiao[1], Y. J. Xiao[1,19], Z. J. Xiao[37], Y. G. Xie[1,7], Y. H. Xie[33], X. A. Xiong[1,19], Q. L. Xiu[1,7], G. F. Xu[1], J. J. Xu[1,19], L. Xu[1], Q. J. Xu[50], X. P. Xu[48], F. Yan[23], L. Yan[5,6], W. B. Yan[7,8], W. C. Yan[62], Y. H. Yan[65], H. J. Yang[26,71], H. X. Yang[1], L. Yang[18], R. X. Yang[7,8], S. L. Yang[1,19], Y. H. Yang[24], Y. X. Yang[54], Yifan Yang[1,19], Z. Q. Yang[65], M. Ye[1,7], M. H. Ye[52], J. H. Yin[1], Z. Y. You[49], B. X. Yu[1,7,19], C. X. Yu[28], J. S. Yu[65], C. Z. Yuan[1,19], Y. Yuan[1], A. Yuncu[21,77], A. A. Zafar[42], Y. Zeng[65], B. X. Zhang[1], B. Y. Zhang[1,7], C. C. Zhang[1], D. H. Zhang[1], H. H. Zhang[49], H. Y. Zhang[1,7], J. Zhang[1,19], J. L. Zhang[66], J. Q. Zhang[4], J. W. Zhang[1,7,19], J. Y. Zhang[1], J. Z. Zhang[1,19], K. Zhang[1,19], L. Zhang[30], S. F. Zhang[24], T. J. Zhang[26,71], X. Y. Zhang[41], Y. Zhang[7,8], Y. H. Zhang[1,7], Y. T. Zhang[7,8], Yang Zhang[1], Yao Zhang[1], Yu Zhang[19], Z. H. Zhang[33], Z. P. Zhang[8], Z. Y. Zhang[18], G. Zhao[1], J. W. Zhao[1,7], J. Y. Zhao[1,19], J. Z. Zhao[1,7], Lei Zhao[7,8], Ling Zhao[1], M. G. Zhao[28], Q. Zhao[1], S. J. Zhao[29], T. C. Zhao[1], Y. B. Zhao[1,7], Z. G. Zhao[7,8], A. Zhemchugov[10,69], B. Zheng[23], J. P. Zheng[1,7], W. J. Zheng[41], Y. H. Zheng[19], B. Zhong[37], L. Zhou[1,7], Q. Zhou[1,19], X. Zhou[18], X. K. Zhou[7,8], X. R. Zhou[7,8], X. Y. Zhou[1], Xiaoyu Zhou[65], Xu Zhou[65], A. N. Zhu[1,19], J. Zhu[28], J. Zhu[49], K. Zhu[1], K. J. Zhu[1,7,19], S. Zhu[1], S. H. Zhu[67], X. L. Zhu[30], Y. C. Zhu[7,8], Y. S. Zhu[1,19], Z. A. Zhu[1,19], J. Zhuang[1,7], B. S. Zou[1] and J. H. Zou[1]

[1]Institute of High Energy Physics, Beijing, China. [2]G.I. Budker Institute of Nuclear Physics SB RAS (BINP), Novosibirsk, Russia. [3]Helmholtz Institute Mainz, Mainz, Germany. [4]Bochum Ruhr-University, Bochum, Germany. [5]University of Turin, Turin, Italy. [6]INFN, Turin, Italy. [7]State Key Laboratory of Particle Detection and Electronics, Beijing, Hefei, China. [8]University of Science and Technology of China, Hefei, China. [9]Southeast University, Nanjing, China. [10]Joint Institute for Nuclear Research, Dubna, Moscow, Russia. [11]INFN Laboratori Nazionali di Frascati, Frascati, Italy. [12]Peking University, Beijing, China. [13]Institute of Physics and Technology, Ulaanbaatar, Mongolia. [14]Indiana University, Bloomington, IN, USA. [15]Carnegie Mellon University, Pittsburgh, PA, USA.

[16]Johannes Gutenberg University of Mainz, Mainz, Germany. [17]INFN Sezione di Ferrara, Ferrara, Italy. [18]Wuhan University, Wuhan, China. [19]University of Chinese Academy of Sciences, Beijing, China. [20]Ankara University, Tandogan, Ankara, Turkey. [21]Istanbul Bilgi University, Eyup, Istanbul, Turkey. [22]Uludag University, Bursa, Turkey. [23]University of South China, Hengyang, China. [24]Nanjing University, Nanjing, China. [25]Lanzhou University, Lanzhou, China. [26]Shanghai Jiao Tong University, Shanghai, China. [27]Liaoning University, Shenyang, China. [28]Nankai University, Tianjin, China. [29]Zhengzhou University, Zhengzhou, China. [30]Tsinghua University, Beijing, China. [31]University of Ferrara, Ferrara, Italy. [32]University of Eastern Piedmont, Alessandria, Italy. [33]Central China Normal University, Wuhan, China. [34]University of Minnesota, Minneapolis, MN, USA. [35]GSI Helmholtzcentre for Heavy Ion Research GmbH, Darmstadt, Germany. [36]Guangxi University, Nanning, China. [37]Nanjing Normal University, Nanjing, China. [38]KVI-CART, University of Groningen, Groningen, The Netherlands. [39]Henan Normal University, Xinxiang, China. [40]University of Hawaii, Honolulu, HI, USA. [41]Shandong University, Jinan, China. [42]University of the Punjab, Lahore, Pakistan. [43]Uppsala University, Uppsala, Sweden. [44]Huangshan College, Huangshan, China. [45]University of Jinan, Jinan, China. [46]University of Muenster, Muenster, Germany. [47]Justus-Liebig-Universitaet Giessen, II Physikalisches Institut, Giessen, Germany. [48]Soochow University, Suzhou, China. [49]Sun Yat-Sen University, Guangzhou, China. [50]Hangzhou Normal University, Hangzhou, China. [51]Beijing Institute of Petrochemical Technology, Beijing, China. [52]China Center of Advanced Science and Technology, Beijing, China. [53]Sichuan University, Chengdu, China. [54]Guangxi Normal University, Guilin, China. [55]Indian Institute of Technology Madras, Chennai, India. [56]Shanxi University, Taiyuan, China. [57]Henan University of Science and Technology, Luoyang, China. [58]Zhejiang University, Hangzhou, China. [59]Fudan University, Shanghai, China. [60]INFN and University of Perugia, Perugia, Italy. [61]COMSATS Institute of Information Technology, Lahore, Pakistan. [62]Beihang University, Beijing, China. [63]Hunan Normal University, Changsha, China. [64]Near East University, Nicosia, North Cyprus, Turkey. [65]Hunan University, Changsha, China. [66]Xinyang Normal University, Xinyang, China. [67]University of Science and Technology Liaoning, Anshan, China. [68]The Novosibirsk State University, Novosibirsk, Russia. [69]The Moscow Institute of Physics and Technology, Moscow, Russia. [70]The Functional Electronics Laboratory, Tomsk State University, Tomsk, Russia. [71]Key Laboratory for Particle Physics, Astrophysics and Cosmology, Ministry of Education; Shanghai Key Laboratory for Particle Physics and Cosmology, Institute of Nuclear and Particle Physics, Shanghai, China. [72]Istanbul Arel University, Istanbul, Turkey. [73]Key Laboratory of Nuclear Physics and Ion-beam Application (MOE) and Institute of Modern Physics, Fudan University, Shanghai, China. [74]Goethe University Frankfurt, Frankfurt, Germany. [75]Government College Women University, Sialkot, Punjab, Pakistan. [76]The NRC 'Kurchatov Institute', PNPI, Gatchina, Russia. [77]Bogazici University, Istanbul, Turkey. *e-mail: andrzej.kupsc@physics.uu.se